Geochemistry Geophysics Geosystems G3
AN ELECTRONIC JOURNAL OF THE EARTH SCIENCES
Published by AGU and the Geochemical Society

Article
Volume 6, Number 11
10 November 2005
Q11004, doi:10.1029/2005GC001006
ISSN: 1525-2027

Formation of the Jinchuan ultramafic intrusion and the world's third largest Ni-Cu sulfide deposit: Associated with the ~825 Ma south China mantle plume?

X. H. Li
Key Laboratory of Isotope Geochronology and Geochemistry, Guangzhou Institute of Geochemistry, Chinese Academy of Sciences, Guangzhou 510640, China (lixh@gig.ac.cn)

Beijing SHRIMP Center, Institute of Geology, Chinese Academy of Geological Sciences, Beijing 100037, China

L. Su
Geological Laboratory Center, China University of Geosciences (Beijing), Beijing 100083, China

S.-L. Chung
Department of Geosciences, National Taiwan University, Taipei 106, Taiwan

Z. X. Li
Tectonics Special Research Centre, School of Earth and Geographical Sciences, University of Western Australia, Crawley, WA 6009, Australia

Y. Liu
Key Laboratory of Isotope Geochronology and Geochemistry, Guangzhou Institute of Geochemistry, Chinese Academy of Sciences, Guangzhou 510640, China

B. Song and D. Y. Liu
Beijing SHRIMP Center, Institute of Geology, Chinese Academy of Geological Sciences, Beijing 100037, China

[1] We report here SHRIMP U-Pb geochronological, geochemical, and Nd isotopic data for the Jinchuan ultramafic intrusion (Gansu Province, China), which hosts the world's third largest magmatic Ni-Cu sulfide deposits. U-Pb baddeleyite analyses yield an age of 812 ± 26 Ma for the ultramafic intrusion. This age is indistinguishable within analytical uncertainties from the U-Pb zircon ages of 827 ± 8 Ma and 828 ± 3 Ma for the sulfide-bearing ultramafic rocks and the dolerite dykes that cut the ultramafic intrusion, respectively. These U-Pb dating results show beyond doubt that the Jinchuan ultramafic intrusion and associated Ni-Cu sulfide deposit were formed at ~825 Ma, rather than ~1500 Ma as has been widely believed. The ultramafic rocks exhibit large negative εNd(T) values (−8.9 to −12.0) that decrease with increasing La/Sm, suggesting that their parental magmas were derived from a long-term enriched lithospheric mantle and experienced crustal contamination. Mineralogical, petrological, and geochemical data all indicate that the Jinchuan intrusion was generated by melting of the enriched lithospheric mantle heated by an anomalously hot plume. The U-Pb ages of ~825 Ma for igneous baddeleyites and zircons and ~900–880 Ma for inherited zircons in the Jinchuan mafic-ultramafic rocks are comparable with those in the Qaidam block and Qilian belt, the western extension of the Qinling belt that was likely derived from northern Yangtze craton. The Jinchuan Ni-Cu sulfide-bearing intrusion, along with coeval regional plume-related mafic dykes and tholeiites, and mafic-ultramafic complexes with associated V-Ti and Ni-Cu-PGE mineralization, is interpreted to be genetically related to the ~825 Ma south China mantle plume.

Components: 8779 words, 11 figures, 3 tables.

Keywords: Jinchuan; ultramafic intrusion; Ni-Cu sulfide deposit; U-Pb age; Nd isotopes; geochemistry.

Index Terms: 1040 Geochemistry: Radiogenic isotope geochemistry; 1065 Geochemistry: Major and trace element geochemistry; 1115 Geochronology: Radioisotope geochronology.

Received 26 April 2005; **Revised** 30 June 2005; **Accepted** 21 July 2005; **Published** 10 November 2005.

Li, X. H., L. Su, S.-L. Chung, Z. X. Li, Y. Liu, B. Song, and D. Y. Liu (2005), Formation of the Jinchuan ultramafic intrusion and the world's third largest Ni-Cu sulfide deposit: Associated with the ~825 Ma south China mantle plume?, *Geochem. Geophys. Geosyst.*, *6*, Q11004, doi:10.1029/2005GC001006.

1. Introduction

[2] The Jinchuan ultramafic intrusion in northern central China is a dyke-like body that contains as much as a half billion tones of Ni-Cu sulfide ore (grading 1.2% Ni and 0.7% Cu [*Chai and Naldrett*, 1992a]), and is ranked the world's third largest magmatic Ni-Cu sulfide deposit [*Naldrett*, 1999]. The intrusion is generally believed to be an ultramafic cumulate from a basaltic magma in a continental rift zone [*Chai and Naldrett*, 1992a, 1992b]. It is enigmatic, however, that such a huge Ni-Cu sulfide deposit was hosted by a small intrusion without any obvious external source for the sulfur.

[3] The age of the intrusion and the deposit is also controversial. *Tang et al.* [1992] first reported a Sm-Nd "isochron" date of 1508 ± 31 Ma for the Jinchuan intrusion and associated Ni-Cu sulfides, which has been widely cited as the formation age of the intrusion by subsequent workers [e.g., *Tang and Li*, 1995; *Naldrett*, 1997, 1999; *Barnes and Tang*, 1999; *Li et al.*, 2004]. More recently, *Li et al.* [2004a] reported a SHRIMP U-Pb zircon age of 827 ± 8 Ma for a sulfide-bearing troctolite sample. The authors argued that the Jinchuan deposit was formed in early Neoproterozoic, rather than Mesoproterozoic. However, in view of the presence of inherent zircons in the intrusion and the potential possibility of subsequent Pb loss, it is not beyond doubt that the youngest zircon age indeed dates the timing of crystallization. In this paper, we report SHRIMP U-Pb baddeleyite and zircon ages and geochemical and Nd isotopic data for the ultramafic rocks and dolerites from Jinchuan. These new data demonstrate that the Jinchuan Ni-Cu sulfide ore-bearing intrusion was crystallized in Neoproterozoic, and might be genetically related to the ~825 Ma mantle plume beneath south China.

2. Geological Setting and Samples

[4] The Jinchuan intrusion is one of a series of mafic to ultramafic bodies located in the Longshoushan Uplift that is a fault-bounded, northwest-striking terrane between the Alax massif (the westernmost part of North China craton) to the north and the northern Qilian Orogenic Belt to the south (Figure 1). It intruded Paleoproterozoic migmatites, gneisses and marbles of the so-called "Longshoushan Group", and was in turn cut by dolerite dykes. The intrusion is northwest-elongated, ~6500 m long and 20–527 m wide, and has a total outcrop area of ~1.34 km^2 [*Tang and Li*, 1995]. The main rock types include dunite, troctolite, lherzolite, plagioclase lherzolite and minor olivine pyroxenite (Figure 2). The intrusion was interpreted as the lower portion of an eroded layered intrusion, a trumpet-shaped linear dyke similar to, but smaller than, the Great Dyke in Zimbabwe [*Chai and Naldrett*, 1992b].

[5] Geochemical samples in this study came from surface traverses across the Jinchuan intrusion, underground orebodies and drill holes. Amongst them, two samples were selected for SHRIMP U-Pb analysis. Sample 03JC01 was collected from a 1.2-m wide dolerite dyke (Figure 2f) that strikes northeasterly and crosscuts the Jinchuan intrusion (Figure 1), which would provide an upper limit for the age of the Jinchuan intrusion. It consists of 60% plagioclase, 35% pyroxene and 5% amphibole. Sample 03JC03 is a plagioclase lherzolite (Figure 2e) from the margin of the intrusion. It is composed of 50% olivine, 25% orthopyroxene, 15% clinopyroxene, 8% plagioclase and minor amount of sulfides, chromite and magnetite. The analyzed ultramafic intrusion and dolerite samples are neither deformed nor metamorphosed.

3. Analytical Methods

[6] Baddeleyite and zircon crystals were separated using both heavy-liquid and magnetic methods under conditions free of contamination. They were then documented with transmitted and reflected light micrographs and cathodoluminescence (CL) images in order to define the internal structures of the grains and to select analysis positions. Measurements of U, Th and Pb in zircons were

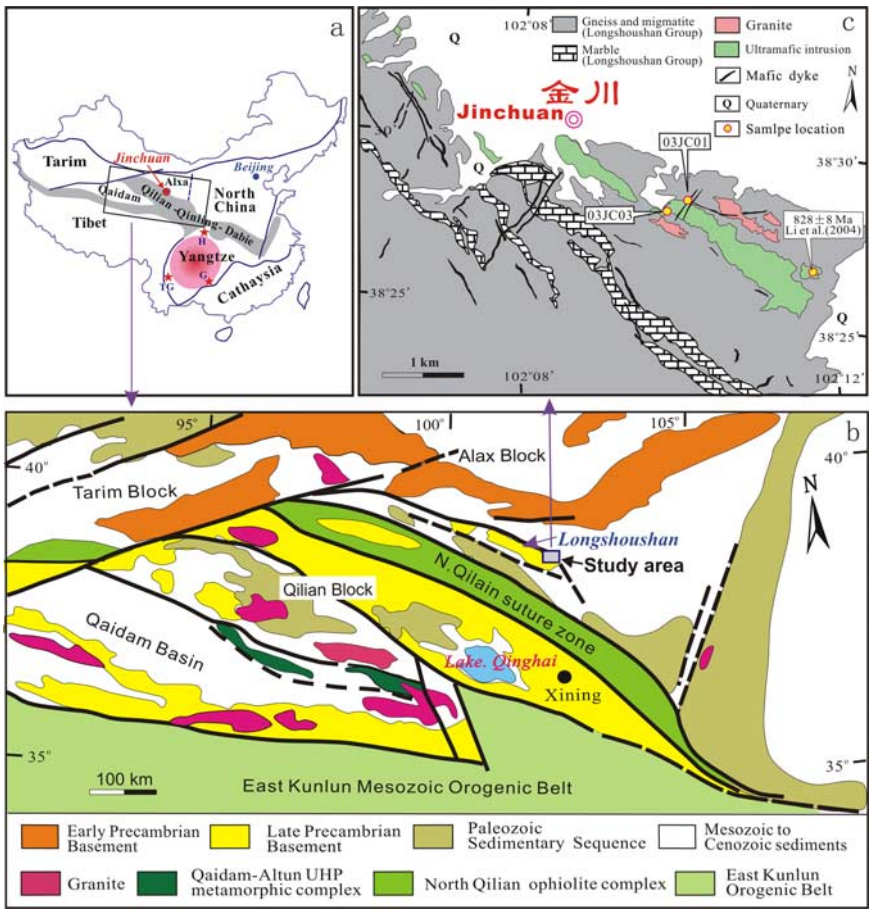

Figure 1. (a) The location of Jinchuan in relation to China's major tectonic units. Red stars show the ~830–820 Ma mafic and ultramafic intrusive rocks of plume origin. G, northern Guangxi mafic dykes and sills [*Li et al.*, 1999]; H, Hannan mafic and ultramafic complex [*Zhou et al.*, 2002; *Su*, 2004]; TG, Tongde-Gaojiacun mafic and ultramafic complex [*Zhu et al.*, 2004]. Dashed line approximates the boundary of the Alxa massif. The pinkish solid circle shows the proposed ~825 Ma south China plume [*Li et al.*, 1999]. (b) Simplified geological map of the western central China showing that the Jinchuan is located between the Alax massif to the north and the northern Qilian Orogenic Belt to the south (modified after *Song et al.* [2003]). (c) Geological map of the Jinchuan region (modified after *SGU* [1984]).

conducted using the SHRIMP II ion microprobe at the Beijing SHRIMP Center, using standard operating conditions [*Williams*, 1998]. U-Th-Pb ratios were determined relative to the TEMROA standard zircon [*Black et al.*, 2003], and the U and Th absolute abundances relative to the SL13 standard zircon. Measured compositions were corrected for common Pb using nonradiogenic ^{204}Pb, and an average crustal composition [*Stacey and Kramers*, 1975] appropriate to the age of the mineral was assumed. U-Pb zircon data are presented in Table 1.

[7] Analyses of baddeleyites were conducted using the SHRIMP II(A) ion microprobe at the Curtin University of Technology. U-Th-Pb ratios and absolute abundances were determined by comparison with the TEMROA and the CZ3 standards, respectively. No correction for Pb isotope discrimination is applied to baddeleyite results [*Wingate et al.*, 1998]. Owing to crystal orientation effects that bias ^{206}Pb/^{238}U ratio measured in baddeleyite by ion microprobe [*Wingate and Compston*, 2000], only ^{207}Pb/^{206}Pb data are reported here (Table 2). Correction of common ^{206}Pb was made using the 208-method [*Compston et al.*, 1984], as this method is more reliable for low ^{232}Th/^{238}U minerals (such as baddeleyite). Accuracy of ^{207}Pb/^{206}Pb for unknowns was monitored by alternating measurements of a baddeleyite reference PBR2 dated at 2060 Ma by both conventional isotope dilution and SHRIMP analysis [*Wingate and Compston*, 2000].

[8] Major element oxides (glass discs) and sulfur (powder pellets) were determined by a Rigaku ZSX100e XRF, and trace elements by a Perkin-Elmer Sciex ELAN 6000 ICP-MS at the Guangzhou

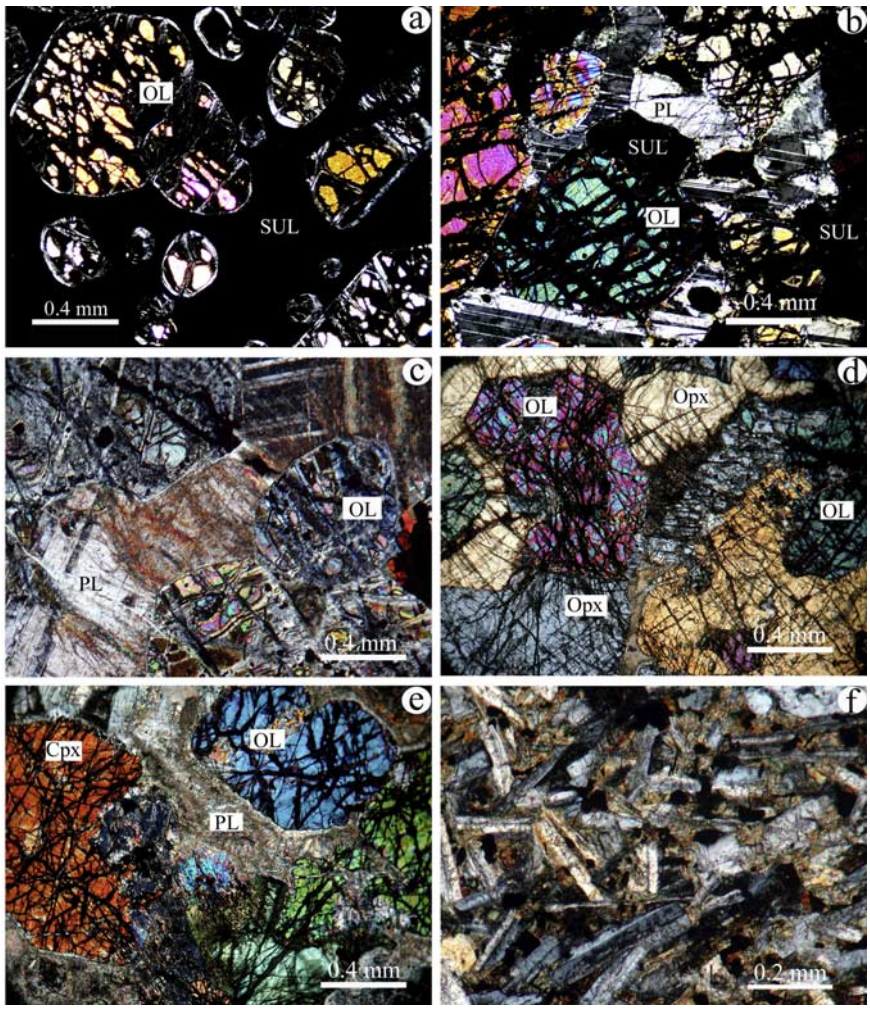

Figure 2. Photomicrographs of the representative lithologies in Jinchuan: (a) sulfide-bearing dunite; (b) sulfide-bearing troctolite (03JC04); (c) coarse-grained troctolite; (d) lherzolite; (e) plagioclase lherzolite (03JC03); (f) dolerite (03JC01).

Institute of Geochemistry. Analytical uncertainties are 1–5% for major elements and <10% for trace elements. Nd isotope analyses were determined using a Micromass Isoprobe multicollector ICP-MS at the same institute, and $^{143}Nd/^{144}Nd$ ratios were adjusted relative to the Shin Etsu JNdi-1 standard of 0.512115. Detailed analytical procedures are given by *Li et al.* [2004b]. Geochemical and Nd isotopic data are listed in Table 3.

4. Analytical Results

4.1. U-Pb Ages

[9] Zircons in sample 03JC01 are mostly euhedral, transparent, 50–100 μm long, and have length/width ratios of ≤2:1. Twenty-seven analyses of 24 zircons were obtained. Eighteen analyses of igneous zircons have variable abundance of Th (114–1713 ppm) and U (120–966 ppm) and Th/U ratio of 0.3–3.1. Their $^{206}Pb/^{238}U$ ratios are in good agreement within analytical errors, and the mean yields an age of 828 ± 3 Ma (95% confidence level) (Figure 3). This age is interpreted as the crystallization age of the dolerite dyke.

[10] Two types of inherited zircons have been identified. The first is rounded, metamorphic zircons showing characteristic radial sector zones in CL image. Amongst the seven inherited metamorphic zircons analyzed, one is discordant, and has $^{207}Pb/^{206}Pb$ age of 1387 ± 34 Ma (1σ), and the others are concordant to slightly discordant with consistent $^{207}Pb/^{206}Pb$ ages between 1807 ± 9 Ma and 1870 ± 19 Ma (1σ). The second is inherited xenocrysts, occurring as either individual crystals or idiomorphic cores with discordant, igneous overgrowth. They usually show distinctly bright

Table 1. SHRIMP U-Pb Zircon Data

Spot	U, ppm	Th, ppm	Th/U	f_{206},[a] %	$^{206}Pb^*/^{238}U$	±1σ	$^{207}Pb^*/^{206}Pb^*$	±1σ	$^{206}Pb^*/^{238}U$ Age, Ma	±1σ	$^{207}Pb^*/^{206}Pb^*$ Age Ma	±1σ
03JC01 (102°10′16.6″E, 38°28′45.1″N)												
1.1	793	1713	2.23	0.17	0.1379	0.0010	0.0656	0.0007	833	6	793	21
2.1	664	224	0.35	0.33	0.1370	0.0011	0.0674	0.0008	828	6	852	24
3.1	169	165	1.01	0.58	0.1813	0.0018	0.0882	0.0016	1074	10	1387	34
3.2	392	1190	3.14	0.27	0.1366	0.0010	0.0664	0.0008	825	6	819	25
4.1	158	133	0.87	0.72	0.1377	0.0015	0.0658	0.0020	832	9	800	63
5.1	265	308	1.20	0.59	0.1367	0.0013	0.0676	0.0014	826	8	858	44
6.1	186	213	1.18	0.62	0.1470	0.0016	0.0676	0.0017	884	9	855	52
7.1	120	119	1.03	0.78	0.1353	0.0013	0.0682	0.0020	818	7	875	59
8.1	579	252	0.45	0.12	0.2958	0.0019	0.1106	0.0005	1670	9	1809	8
9.1	234	287	1.27	0.43	0.1373	0.0011	0.0671	0.0011	830	6	842	36
10.1	556	180	0.33	0.27	0.1372	0.0009	0.0690	0.0007	829	5	898	21
11.1	546	495	0.94	0.22	0.1470	0.0011	0.0682	0.0008	884	6	875	22
12.1	502	246	0.51	0.10	0.3285	0.0024	0.1144	0.0013	1831	12	1870	19
13.1	258	148	0.59	1.47	0.1393	0.0012	0.0653	0.0019	841	7	786	60
14.1	1296	296	0.24	0.07	0.3247	0.0022	0.1133	0.0004	1812	11	1854	7
15.1	966	258	0.28	0.32	0.1388	0.0009	0.0677	0.0005	838	5	859	17
16.1	550	636	1.19	0.20	0.1376	0.0010	0.0693	0.0007	831	5	906	21
17.1	148	114	0.80	1.64	0.1343	0.0134	0.0702	0.0037	812	8	933	110
17.2	487	463	0.98	0.65	0.1367	0.0010	0.0672	0.0011	826	6	843	34
18.1	191	174	0.94	1.00	0.1352	0.0013	0.0693	0.0020	818	7	907	60
19.1	812	825	1.05	0.25	0.1370	0.0009	0.0676	0.0006	828	5	856	18
20.1	146	124	0.88	1.87	0.1380	0.0015	0.0713	0.0034	833	8	967	96
20.2	176	204	1.20	0.62	0.1377	0.0012	0.0683	0.0014	832	7	878	41
21.1	172	63	0.37	0.69	0.2904	0.0028	0.1110	0.0014	1643	14	1816	23
22.1	554	145	0.27	0.09	0.3243	0.0023	0.1105	0.0005	1811	11	1807	9
23.1	759	302	0.41	0.33	0.1363	0.0009	0.0668	0.0009	824	5	831	27
24.1	330	134	0.42	0.24	0.3240	0.0024	0.1121	0.0009	1809	12	1833	14
03JC03 (102°10′08.4″E, 38°28′37.7″N)												
1.1	331	520	0.66	0.66	0.1494	0.0014	0.0735	0.0017	897	8	1027	46
2.1	426	1410	0.63	0.63	0.1477	0.0013	0.0700	0.0014	888	8	928	42
3.1	420	1353	0.60	0.60	0.1499	0.0013	0.0674	0.0013	900	8	851	39
4.1	246	635	0.58	0.58	0.1441	0.0014	0.0681	0.0016	868	8	870	47
5.1	74	88	1.99	1.99	0.2928	0.0041	0.1145	0.0041	1655	20	1873	65

[a] f_{206} is the percentage of common ^{206}Pb in total ^{206}Pb.

concentric CL images in contrast to those ~828 Ma magmatic zircons that have relatively dark CL images. Two analyses of xenocryst zircons yield identical $^{206}Pb/^{238}U$ ages of ~884 Ma, similar to the ~880 Ma ages of xenocryst zircons from a previous study (sample 03JC04 [*Li et al.*, 2004a]).

[11] Baddeleyite crystals, separated from a 30 kg sample 03JC03, are euhedral, stubby (30–50 μm long) and have length/width ratios of ≤2:1. Twenty-one analyses were made, one on each baddeleyite crystal. The analyzed baddeleyites have variably low U; nineteen grains have U < 100 ppm, and other two have U = 153–212 ppm. They are extremely low in Th, ranging from <1 ppm to 7.5 ppm, characteristic of baddeleyite, because Th^{4+} has larger ionic radius and apparently does not substitute for Zr^{4+} as preferably for U^{4+}. Th/U ratios are all lower than 0.1. The $^{207}Pb^*/^{206}Pb^*$ ages are determined with variably low precisions, and they are all indistinguishable within analytical uncertainties. Errors on ages calculated from individual analyses reported here range from ±27 Ma to ±240 Ma (1σ). The low precision is a consequence of the insensitivity of the $^{207}Pb^*/^{206}Pb^*$ ratios as a measure of age in Neoproterozoic and younger rocks, and the low abundance of radiogenic ^{207}Pb in the analyzed baddeleyites with low U concentration. All measured $^{207}Pb^*/^{206}Pb^*$ ratios form a single, approximately Gaussian population (Figure 4), and the weighted mean yields an age of 812 ± 25 Ma (95% confidence level). This age is interpreted as the crystallization age of the Jinchuan ultramafic intrusion and thus the large Ni-Cu sulfide deposit (see discussion later).

Table 2. SHRIMP U-Pb Baddeleyite Data for 03JC03 Baddeleyite[a]

Spot	U, ppm	Th, ppm	Th/U	f_{206}, %	$^{207}Pb^*/^{206}Pb^*$	±1σ	$^{207}Pb^*/^{206}Pb^*$ Age, Ma	±1σ
1.1	42	1.0	0.025	1.67	0.0662	0.0023	813	73
2.1	52	1.4	0.029	3.50	0.0648	0.0038	770	120
3.1	49	1.3	0.027	0.47	0.0664	0.0021	818	65
4.1	47	0.9	0.020	1.73	0.0644	0.0022	755	72
5.1	48	0.9	0.019	0.91	0.0644	0.0021	756	68
6.1	49	2.0	0.043	2.35	0.0671	0.0029	840	100
7.1	46	2.1	0.047	8.62	0.0667	0.0033	830	99
8.1	53	0.9	0.017	1.06	0.0705	0.0019	943	53
9.1	39	1.0	0.027	3.87	0.0643	0.0073	750	240
10.1	63	0.7	0.011	0.70	0.0659	0.0031	800	100
11.1	48	3.1	0.066	5.49	0.0668	0.0057	830	180
12.1	96	4.8	0.052	1.59	0.0692	0.0025	905	74
13.1	86	4.3	0.052	0.38	0.0642	0.0014	750	46
14.1	37	1.2	0.032	1.12	0.0686	0.0023	880	68
15.1	75	2.7	0.037	1.85	0.0656	0.0015	792	48
16.1	40	0.9	0.023	3.04	0.0620	0.0019	675	66
17.1	153	5.2	0.035	0.65	0.0667	0.0021	828	65
18.1	39	0.7	0.018	1.88	0.0655	0.0018	791	57
19.1	51	0.8	0.017	1.17	0.0664	0.0020	818	63
20.1	80	1.8	0.023	0.84	0.0649	0.0013	771	42
21.1	212	7.5	0.037	0.28	0.0671	0.0009	841	27

[a] U and Th contents are approximate but proportional to true values.

[12] Less than ten zircon grains were recovered from the same sample (03JC03), and they all are inherited zircons as shown by their CL image characters. One rounded, inherited metamorphic zircon is discordant, and has $^{207}Pb/^{206}Pb$ age of 1873 ± 65 Ma (1σ), whereas the other four xenocryst zircons are concordant, and have $^{206}Pb/^{238}U$ ages between 868 ± 8 Ma and 900 ± 8 Ma (1σ) (Figure 5).

4.2. Geochemical and Nd Isotopic Characteristics

[13] The ultramafic intrusive rocks are very high in MgO and low in TiO_2, Al_2O_3, CaO Na_2O and K_2O. CaO decreases with increasing MgO, following the compositional trend dominantly controlled by olivine accumulation (Figure 6a). In the Pearce element ratio diagram of (Mg + Fe)/Al versus Si/Al (Figure 6b), the data forms a linear regression line with a slope of 2.04, close to the ideal index of 2.0 for crystal addition/separation of olivine [*Russell and Nicholls*, 1988]. It is noted that these rocks underwent variably hydrothermal alteration and serpentinized at relatively low temperatures. Such an alteration process might change not only those chemically mobile elements, such as Na, K and the large ion lithosphile (LIL) elements, but also some relatively immobile elements, such as REE of ultramafic rocks [e.g., *Gruau et al.*, 1998; *Chen et al.*, 2002]. For evaluating the change of chemical compositions during the alteration process, a few elements of different geochemical behaviors, K_2O, Rb, Nb and Sm/Nd, are plotted against LOI (loss of ignition) in Figure 7. Despite somewhat scattered datum points, K_2O and Rb decrease with increasing LOI, indicating that the alkaline and LIL elements were mobile and lost to varying degrees during the alteration. On the contrary, Nb and Sm/Nd are not correlated with LOI, suggesting that the high-field-strength elements and REE are essentially immobile during the alteration. Thus only the immobile elements are used in the following discussion on the petrogenesis of the Jinchuan intrusion. In contrast to the ultramafic rocks, two dolerite samples are fairly fresh as shown by their petrographic features and relatively low LOI values (Table 3).

[14] The major and trace element results (Table 3) suggest that the two dolerite samples (03JC01 and 03JC02) have chemical compositions of tholeiitic basalts, characterized by relatively flat chondrite-normalized REE patterns (La_N = 17–18, $La_N/Sm_N \approx 1.2$) and primitive mantle-normalized incompatible trace element spidergrams with clear Nb-Ta depletion relative to La (Nb/La = 0.53–0.59) (Figure 8).

Table 3. Geochemical and Nd Isotopic Data[a]

Sample	03JC04-2	JC-23	03JC04-1	JC-25	JC-3	JC-4	JC-27	03JC04-3	JC-22	03JC03-1	03JC03-2	JC-31	03JC01	03JC02
Rock type	S-Dun	S-Dun	S-Tro	S-Tro	Dun	Dun	Dun	Lh	Lh	Pl-Lh	Pl-Lh	Pl-Lh	Dol	Dol
							Major Elements, %							
SiO_2	35.23	35.27	42.59	37.51	37.41	37.29	39.17	36.39	37.07	39.93	40.02	43.89	48.75	48.40
TiO_2	0.24	0.29	0.38	0.26	0.19	0.24	0.39	0.27	0.25	0.25	0.37	0.63	0.90	0.87
Al_2O_3	1.81	3.50	4.88	5.16	1.89	2.42	4.01	2.55	3.09	3.00	5.75	7.95	14.17	11.53
$Fe_2O_3^T$	19.53	17.72	14.46	14.59	13.33	13.44	13.28	11.42	14.38	13.06	13.85	12.14	11.57	11.23
MnO	0.18	0.14	0.17	0.18	0.15	0.16	0.15	0.10	0.10	0.15	0.18	0.17	0.19	0.18
MgO	33.96	27.76	27.24	25.30	36.34	35.22	32.70	33.99	31.23	31.03	26.87	24.63	7.67	7.36
CaO	1.62	2.59	4.11	3.38	0.73	1.13	2.24	1.23	1.37	2.01	4.00	5.04	12.46	14.91
Na_2O	0.10	0.21	0.70	0.36	0.11	0.18	0.53	0.07	0.16	0.13	1.11	1.06	3.07	2.50
K_2O	0.20	0.02	0.27	0.21	0.04	0.06	0.26	0.04	0.10	0.15	0.43	0.63	1.05	0.75
P_2O_5	0.00	0.04	0.02	0.04	0.03	0.03	0.06	0.06	0.03	0.01	0.04	0.08	0.03	0.05
LOI	3.25	7.04	3.45	7.74	8.39	8.92	6.57	13.52	10.24	10.73	7.12	3.61	0.12	2.31
Total	96.12	94.58	98.27	94.73	98.61	99.09	99.36	99.64	98.02	100.45	99.74	99.83	99.96	100.09
Mg#	0.80	0.81	0.80	0.81	0.84	0.84	0.83	0.81	0.81	0.82	0.80	0.80	0.57	0.56
S	3.34	3.57	0.97	3.93	0.20	0.14	0.18	0.21	0.20	0.09	0.48	0.14	0.12	0.09
							Trace Elements, ppm							
Cr	3146	3208	3341	3200	7197	4473	6195	4479	5103	4800	3192	2700	136	134
Co	262	404	144	239	133	135	131	132	190	122	118	109	45	38
Ni	6945	11266	2202	6533	1277	1186	1003	1179	4107	1045	1855	807	84	75
Cu	5114	3950	1318	11313	25	44	94	43	1250	25	169	77	76	65
Zn	102	89	81	147	95	83	106	90	90	71	117	78	114	100
Ga	8.8	9.3	10.6	10.3	8.3	8.0	9.0	8.4	10.2	9.1	11.1	12.3	15.0	15.7
Rb	6.48	1.22	6.69	8.10	1.13	1.00	3.86	1.04	6.58	3.60	16.57	22.0	23.2	16.0
Sr	48.9	28.5	203	52.5	18.8	44.4	30.2	21.9	60.8	161	110	282	303	241
Y	5.30	5.64	7.93	6.94	2.82	3.20	4.12	4.33	6.44	4.48	7.98	12.54	19.12	18.90
Zr	33.6	29.8	35.9	39.0	14.6	18.0	16.0	30.5	31.7	25.2	46.9	74.5	62.9	50.4
Nb	2.81	2.53	2.92	2.77	2.01	2.16	2.15	2.54	2.98	2.26	2.97	4.17	2.49	2.11
Ba	185	24.0	109	103	47.2	81.4	147	30.8	264	47.1	264	602	2059	1210
La	3.64	2.63	4.92	3.71	2.61	3.17	2.56	3.17	3.85	2.95	7.26	10.6	4.25	3.95
Ce	7.32	6.84	9.88	9.07	4.84	5.74	5.55	6.06	8.81	5.93	13.52	21.5	10.5	9.94
Pr	0.88	0.93	1.19	1.15	0.53	0.63	0.67	0.73	1.11	0.74	1.44	2.39	1.53	1.43
Nd	3.72	3.96	5.24	4.80	1.94	2.38	2.72	3.22	4.65	3.32	5.92	9.75	8.03	6.50
Sm	0.89	0.97	1.33	1.21	0.52	0.60	0.70	0.84	1.11	0.86	1.36	2.28	2.30	2.05
Eu	0.25	0.29	0.41	0.39	0.16	0.20	0.24	0.21	0.32	0.26	0.46	0.73	0.85	0.68
Gd	0.90	0.94	1.38	1.17	0.49	0.59	0.71	0.75	1.01	0.78	1.34	2.22	3.11	2.74
Tb	0.15	0.16	0.23	0.20	0.08	0.10	0.12	0.12	0.18	0.13	0.23	0.38	0.54	0.49
Dy	0.91	0.96	1.38	1.17	0.49	0.58	0.72	0.73	1.14	0.78	1.37	2.16	3.50	3.11
Ho	0.19	0.20	0.29	0.25	0.10	0.12	0.15	0.15	0.24	0.17	0.30	0.47	0.73	0.66
Er	0.54	0.55	0.80	0.71	0.28	0.33	0.42	0.42	0.64	0.45	0.82	1.29	1.85	1.86
Tm	0.08	0.09	0.12	0.10	0.04	0.05	0.07	0.06	0.09	0.07	0.13	0.20	0.30	0.28

Table 3. (continued)

Sample	03JC04-2	JC-23	03JC04-1	JC-25	JC-3	JC-4	JC-27	03JC04-3	JC-22	03JC03-1	03JC03-2	JC-31	03JC01	03JC02
Rock type	S-Dun	S-Dun	S-Tro	S-Tro	Dun	Dun	Dun	Lh	Lh	Pl-Lh	Pl-Lh	Pl-Lh	Dol	Dol
Yb	0.51	0.52	0.75	0.65	0.28	0.31	0.41	0.39	0.59	0.42	0.78	1.19	2.07	1.81
Lu	0.08	0.08	0.11	0.10	0.04	0.05	0.06	0.05	0.08	0.06	0.11	0.17	0.34	0.28
Hf	0.75	0.71	0.86	0.94	0.35	0.43	0.39	0.63	0.74	0.55	1.04	1.64	1.75	1.35
Ta	0.16	0.15	0.17	0.18	0.12	0.13	0.13	0.15	0.18	0.14	0.17	0.25	0.15	0.13
Th	0.49	0.41	0.53	0.57	0.28	0.32	0.31	0.37	0.39	0.37	0.61	0.96	0.30	0.22
U	0.08	0.06	0.09	0.09	0.04	0.06	0.30	0.08	0.08	0.05	0.10	0.14	0.12	0.13
$^{147}Sm/^{144}Nd$	0.145	0.149	0.153	0.153	0.161	0.153	0.157	0.157	0.144	0.156	0.139	0.141	0.173	0.191
$^{143}Nd/^{144}Nd$	0.511851	0.511910	0.511897	0.511942	0.511830	0.511815	0.511889	0.511881	0.511885	0.511917	0.511772	0.511823	0.512292	0.512293
$\pm 2\sigma_m$	0.000013	0.000015	0.000013	0.000014	0.000015	0.000014	0.000014	0.000014	0.000014	0.000014	0.000013	0.000013	0.000012	0.000016
εNd(T)	−9.9	−9.1	−9.9	−8.9	−12.0	−11.4	−10.3	−10.6	−9.1	−9.8	−10.8	−10.1	−4.3	−6.1

S-Dun, sulfide-bearing dunite; S-Tro, sulfide-bearing troctolite; Dun, dunite; Lh, Lherzolite; Pl-Lh, plagioclase Lherzolite; Dol, dolerite.
[a] $Mg\# = Mg/(Mg + Fe^{2+})$, assuming $Fe_2O_3/(FeO + Fe_2O_3) = 0.20$. Total iron as Fe_2O_3. T = 827 Ma.

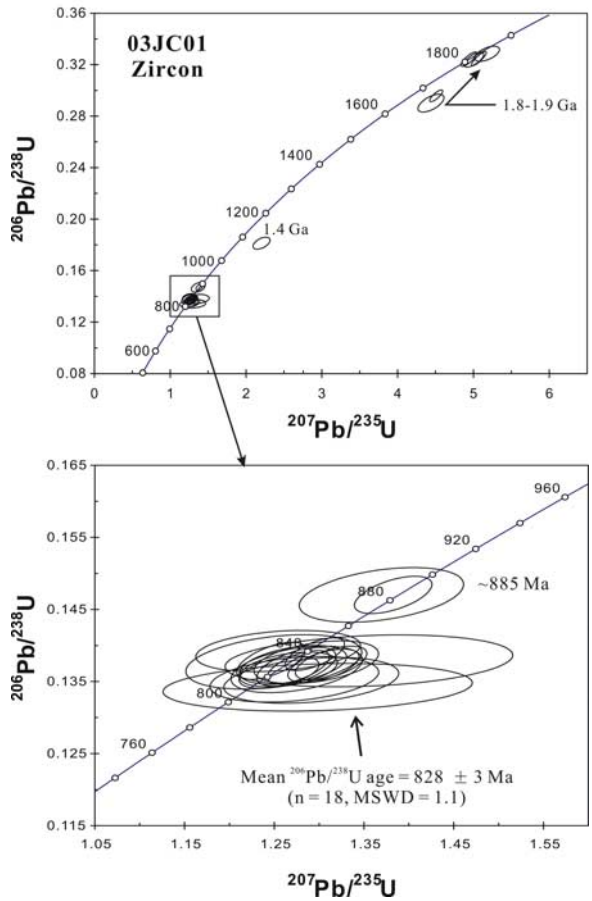

Figure 3. Concordia plot of SHRIMP U-Pb zircon results for dolerite sample 03JC01 from Jinchuan (MSWD, mean square of weighted deviates).

[15] The ultramafic rocks have variable abundances in REE and other trace elements due to varying degrees of olivine accumulation. They generally display similar REE and trace element patterns (Figure 8). Compared with the dolerites, the ultramafic rocks have steeper, LREE/HREE fractionated patterns (La_N/Sm_N = 1.8–3.5), with a few samples having even higher LREE abundance. Although they exhibit varying degrees of Nb and Ta depletion relative to Th and La (Nb/La = 0.39–0.96), their geochemical compositions generally share affinities to those of basaltic rocks formed in intraplate settings (Figure 9), rather than arcs.

[16] The ultramafic rocks have a limited range of $^{147}Sm/^{144}Nd$ ratios between 0.14 and 0.16, and the calculated εNd(T) values (T = 825) range from −8.9 to −12.0. On the other hand, the dolerite samples have relatively high $^{147}Sm/^{144}Nd$ ratio of 0.17–0.19 and initial εNd(T) values of −4.3 to −6.1. Negative εNd(T) values exclude a depleted

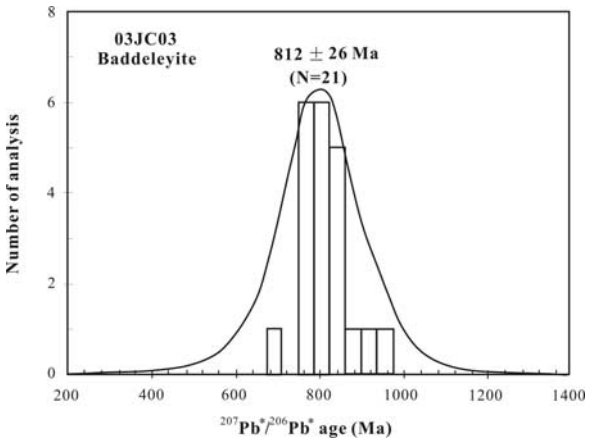

Figure 4. Histogram of SHRIMP baddeleyite $^{207}Pb^*/^{206}Pb^*$ ages for plagioclase lherzolite sample 03JC03 from the Jinchuan intrusion.

asthenosphere mantle as a sole source for both the ultramafic intrusive rocks and the dolerite dykes.

5. Discussion

5.1. Age of the Jinchuan Intrusion

[17] The SHRIMP U-Pb zircon age of 828 ± 3 for the dolerite dyke sample 03JC01 provides a minimal age for the formation of the main body of the Jinchuan intrusion, as the dyke crosscuts the ultramafic intrusion.

[18] Baddeleyite is ideal for dating the crystallization of mafic intrusions by the U-Pb method, because it crystallizes in the late-stage, chemically fractionated portions of mafic magmas, it rarely occurs as xenocrysts in mafic intrusion, and appears to be less susceptible to Pb loss than zircon [*Heaman and LeCheminant*, 1993]. Our SHRIMP U-Pb baddeleyite analyses suggest that the main body of the Jinchuan intrusion was crystallized at 812 ± 26 Ma, indistinguishable within errors with the minimal age of 828 ± 3 Ma provided by the crosscutting dyke. Our new SHRIMP U-Pb ages are in good agreement within errors with a new Re-Os isochron age of 852 ± 25 Ma [*Yang et al.*, 2004] and a new concordant SHRIMP U-Pb zircon age of 827 ± 8 Ma for a sulfide-bearing troctolite sample in our previous work [*Li et al.*, 2004a]. This troctolite sample (Figure 2b) came from the western branch of the underground number 2 Ore Body in the easternmost portion of the Jinchuan intrusion; no younger dolerite dykes occur to its proximity. Thus it could not have been affected by the dolerite emplacement. The igneous zircons dated at 827 ± 8 Ma from this sample show wide CL concentric zoning without any subsequent overgrowth rim. They have distinctively high

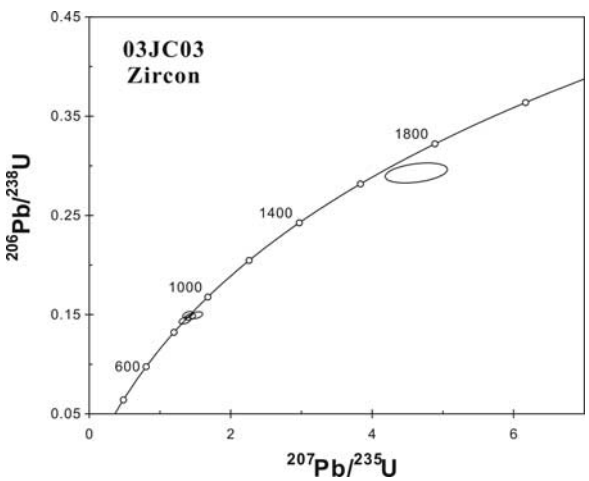

Figure 5. Concordia plot of SHRIMP U-Pb zircon results for the plagioclase lherzolite sample 03JC03 from the Jinchuan Intrusion.

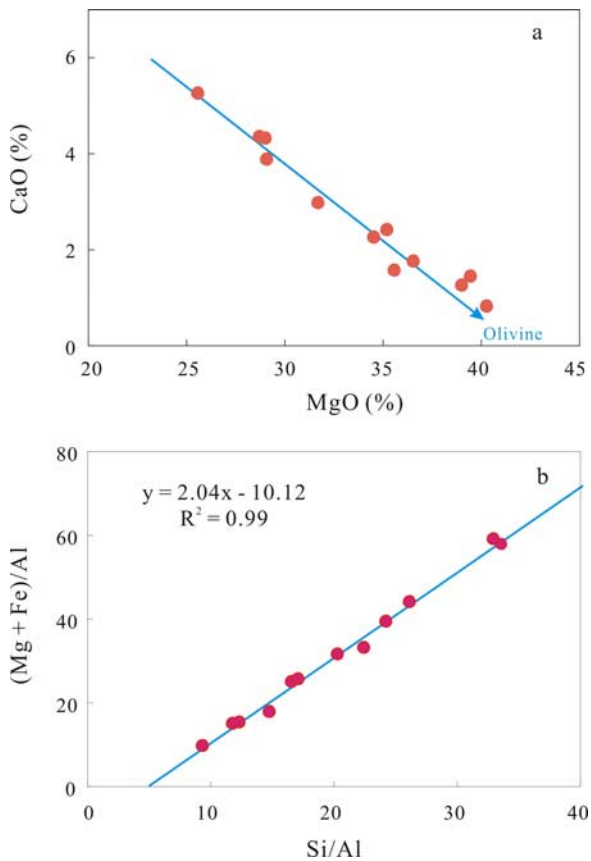

Figure 6. (a) CaO versus MgO plot and (b) the Pearce element ratio diagram of (Mg + Fe)/Al versus Si/Al for the ultramafic rocks, illustrating that the major chemical compositions of the Jinchuan intrusion are dominantly controlled by olivine accumulation.

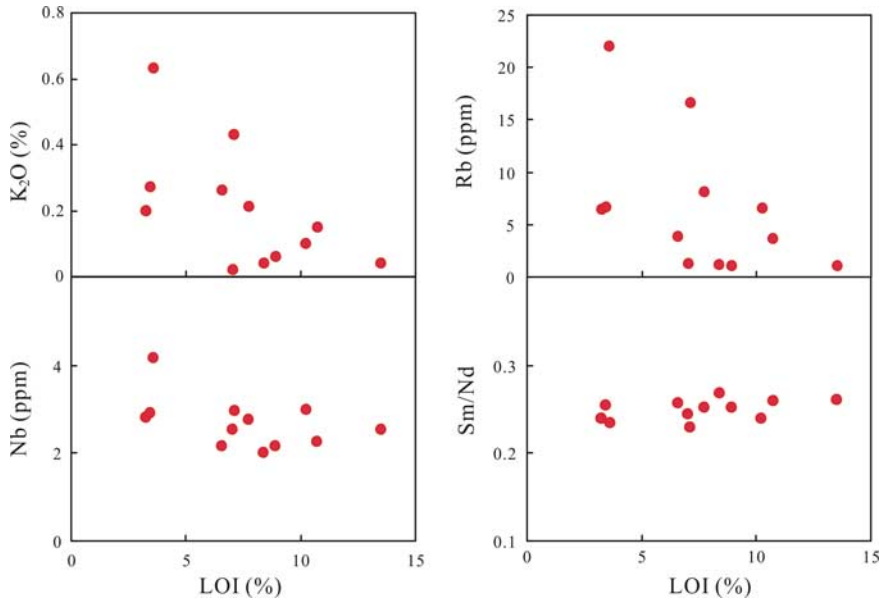

Figure 7. Plot of K_2O, Rb, Nb, and Sm/Nd versus LOI for the ultramafic rocks to evaluate the mobility of the alkaline, LIL, HSF, and rare earth elements during alteration processes.

Th/U ratios, mostly between 3 and 6 with the highest up to 15.9, characteristic of zircons crystallized in mafic melts. Thus we conclude that the Jinchuan ultramafic intrusion and associated Ni-Cu sulfide deposits were formed at ~825 Ma.

[19] It should be pointed out that the aforementioned new age results are at dart contrast to the widely accepted Sm-Nd "isochron age" of 1508 ± 31 Ma [*Tang et al.*, 1992]. This Sm-Nd date is highly problematic, because the Sm-Nd "isochron" is more likely an errorchron or a binary mixing line in view of the limited range of $^{147}Sm/^{144}Nd$ ratios (0.122–0.160) and a negative intercepted εNd(T) value (−3.7) for the analyzed samples.

5.2. Magma Genesis

[20] There is a general consensus that the currently exposed Jinchuan intrusion represents only a small part, probably 2–3%, of the magmas emplaced, and the majority of the latter were eroded [*Chai and Naldrett*, 1992a, 1992b; *Li et al.*, 2004]. *Chai and Naldrett* [1992b] suggested that the parental magma of the Jinchuan intrusion was a high-Mg tholeiite formed by high degree melting of the mantle. In view of the pronounced negative εNd(T) values as well as variable Nb-Ta depletions relative to La (Figure 8), crustal materials appeared to have been incorporated in the Jinchuan ultramafic rocks. There is a tight negative correlation between εNd(T) value and La/Sm ratio for these rocks (Figure 10), indicating that the variable negative εNd(T) values were attributed to the crustal contamination during the formation of the intrusion. This interpretation is supported by a

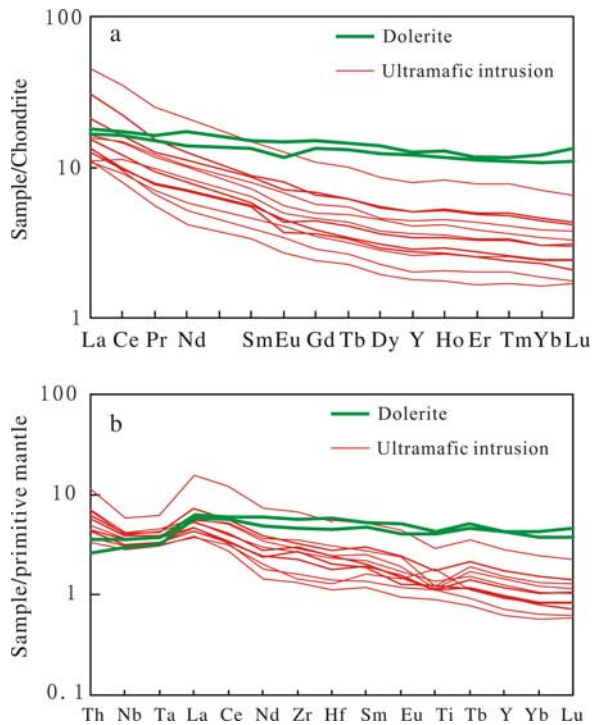

Figure 8. (a) Chondrite-normalized REE patterns and (b) primitive mantle-normalized incompatible trace element spidergrams for the Jinchuan ultramafic rocks and dolerites. Normalizing values from *Sun and McDonough* [1989].

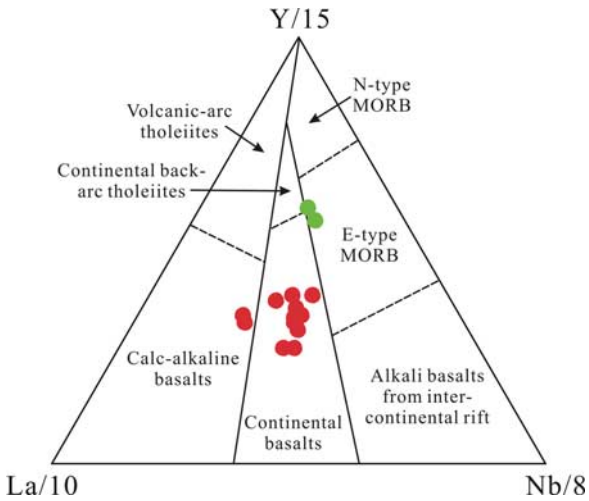

Figure 9. The La-Y-Nb diagram for basaltic rocks formed in distinct tectonic environments [after *Cabanis and Lecolle*, 1989]. The Jinchuan mafic-ultramafic rocks display clearly different geochemical characteristics from those of arc basaltic rocks. The ultramafic rocks plot mostly into the field of continental basalts, whereas the dolerite dykes seem to be more akin to the E-type MORB. The red and green dots represent the ultramafic and dolerite samples, respectively.

recent study of sulfide Re-Os isotopes by *Yang et al.* [2004] who reported a Re-Os isochron age of 852 ± 25 Ma with a high initial $^{187}Os/^{188}Os$ ratio of 0.255 (corresponding to a γOs(T) value of +110). Consistency between the Re-Os sulfide age and U-Pb zircon and baddeleyite ages for Jinchuan ultramafic rocks implies a closed Re-Os isotopic system since its formation. Therefore the intercepted $^{187}Os/^{188}Os$ ratio indeed represents the Os isotopic composition of the magma, which is much higher than $^{187}Os/^{188}Os$ values of all known mantle reservoirs [*Shirey and Walker*, 1998]. The only reservoir known to contain significant radiogenic Os is old continental crust [*Chesley and Ruiz*, 1998]. Therefore the Os isotopic composition does not reflect a primary mantle composition. Instead, the crustal materials must have been involved in the genesis of the Jinchuan intrusion. Assuming the "uncontaminated" parental tholeiitic magma has a less enriched and relatively flat REE pattern with La/Sm ≈ 2.5, its εNd(T) value can be very well estimated at approximately −8 by extrapolation from the correlation between La/Sm and εNd(T) (Figure 10), suggesting that the parental magma was most likely derived from a long-term enriched SCLM source.

[21] Mechanisms to explain crustal components involved in the mantle-derived mafic rocks usually include the magma mixing and the assimilation-fractional crystallization (AFC) processes. Considering that some of the mobile elements analyzed were changed during subsequent alteration processes, we constrained the quantification to REE and Nd isotopic compositions using the binary mixing and the AFC model [*DePaolo*, 1981]. Because the geochemical and isotopic compositions of the regional continental crust are unknown, we use the Archean-Paleoproterozoic basement rocks from the northern Yangtze craton (rather than the North Chian craton, see discussion below) as the contaminant crustal components. The

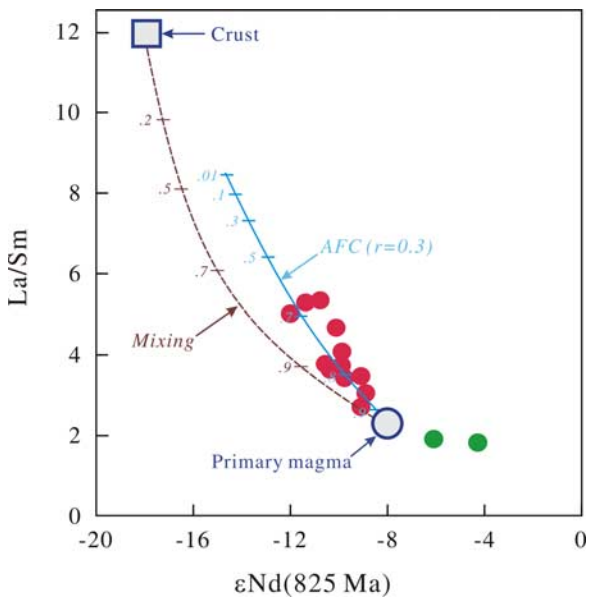

Figure 10. Plot of εNd(T) versus La/Sm for the Jinchuan ultramafic rocks and dolerites. The blue and brown curves represent assimilation-fractional crystallization (AFC) and binary mixing models for the Jinchuan ultramafic rocks, respectively. Numbers labeled on the AFC curve are the instantaneous mass fraction of the melt, and those labeled on the mixing curve are the fraction of the mantle-derived magma. The value of r is the rate of assimilation/rate of crystallization. The crustal compositions (La = 60 ppm, Sm = 5 ppm, Nd = 38 ppm, εNd(827 Ma) = −18) are the average of the metasedimentary rocks from the Archean-Paleoproterozoic Kongling Group in the northern Yangtze craton [*Gao et al.*, 1999]. The primary magmas are assumed having La = 8 ppm, Sm = 3.4 ppm, Nd = 12.8 ppm, similar to the average compositions of the Hawaii picrites [*Norman and Garcia*, 1999], and εNd(827 Ma) = −8. Because the chemical compositions of the Jinchuan intrusion are dominantly controlled by olivine accumulation, the partition coefficients between olivine and melt are used for the fractional crystallization: $D^{La} = 0.0001$, $D^{Nd} = 0.0002$, and $D^{Sm} = 0.0003$ [*McKenzie and O'Nions*, 1991]. Symbols are the same as in Figure 9.

REE compositions of the Jinchuan primary magma are considered to be similar to those of the plume-derived picrites (see discussion below), thus the average compositions of the Hawaiian picrites are used to approximate the Jinchuan primary magma. The calculation results are shown in Figure 10. It is apparent that the binary mixing path is inconsistent with the compositional variations of the ultramafic rocks. In contrast, the AFC path fits the relatively steep trend of the La/Sm-εNd variations. It should be noted that the AFC curve in Figure 10 is the compositional path of the evolving magma, whereas the analyzed rocks are olivine-dominated cumulates that crystallized from the magma. Although the analyzed rocks have much lower REE contents than the instantaneous melt from which they crystallized owing to olivine accumulation, both of them have the same La/Sm and εNd values. In other words, the ultramafic rocks share the same compositional path with the evolving magma. Thus we conclude that the AFC processes can most reasonably explain the geochemical and Nd isotopic data of the Jinchuan intrusion.

[22] On the basis of the composition of olivine, the dominant cumulus mineral in the Jinchuan ultramafic rocks, a modeled composition with MgO = 12% was obtained for the parental magma by *Chai and Naldrett* [1992b]. However, taken the aforementioned crustal contamination into account, the modeled MgO contents of 12% should in fact represent an estimate for the "contaminated magmas" from which the olivine crystallized. In other words, the "uncontaminated" parental magma must have had MgO content exceeding 12%. An investigation of mineral chemistry by *Barnes and Tang* [1999] showed that chromites from the Jinchuan intrusion are highly enriched in Ti, a feature typical of tholeiitic layered intrusions associated with the Karoo flood basalts. These integrated mineralogical, petrological and geochemical data are all consistent with the presence of a mantle plume with $T_p > 1350°C$ [*McKenzie and Bickle*, 1988] for the generation of the Jinchuan intrusion, i.e., the Jinchuan parental magma having MgO contents in excess of 12% was generated by high degree melting of the SCLM heated by an anomalously hot, mantle plume at ~825 Ma.

[23] The dolerites are slightly younger than, but generally coeval with the ultramafic rocks as indicated by their field relationship and the consistent U-Pb zircon ages. Their relatively higher εNd(T) values of −4.3 to −6.1 suggest that they could not be derived solely from the same SCLM source. Instead, their parental magma might be stemmed from either a depleted asthenospheric mantle, or an OIB-type mantle plume. The dolerite samples exhibit geochemical affinities to the E-type MORBs as shown by their relatively flat REE patterns and slightly enrichment in most incompatible trace elements (Figure 8b). In the La-Y-Nb discrimination diagram of *Cabanis and Lecolle* [1989], they plot into the E-type MORB field (Figure 9). In addition, they show variable enrichment in LIL elements, such as Rb (16–23 ppm), Sr (241–303 ppm) and Ba (1210–2059 ppm). All these geochemical and Nd isotopic characters are consistent with the involvement of enriched lithospheric mantle components, rather than crustal materials, in the asthenosphere- or plume-derived magma. We noticed that these two dolerite samples have Fe/Mn ratios = 68–69, which are consistent to those of the Hawaiian OIB (Fe/Mn = 65–71), but higher than those of MORB and mantle peridotites that usually have relatively low Fe/Mn ratios of approximately ≤60 [*Humayun et al.*, 2004]. Despite the dissension on genesis of excess Fe in the Hawaiian OIB [*Humayun et al.*, 2004; *Lee*, 2004], it seems that the plume-derived magmas are characterized by high Fe/Mn ratio. Therefore we are tentatively apt to favor a plume origin for the Jinchuan dolerite. This plume likely caused remelting of the overlying SCLM to form the Jinchuan ultramafic intrusion. Further investigations are needed for the petrogenesis of these dolerites.

5.3. Implications for Ore Genesis and Tectonic Reconstruction

[24] The vast amount of sulfide accumulation in a small ultramafic body with no obvious adjacent external source for sulfur is an enigmatic feature of the Jinchuan deposit. Values of $\delta^{34}S$ in the Jinchuan sulfides are between −2.6‰ and 3.1‰ [*Sixth Geological Unit of the Gansu Geological Survey* (*SGU*), 1984], which are not diagnostic in constraining the origin of the sulfur. Our geochemical and Nd isotopic data as well as the Os isotopic compositions [*Yang et al.*, 2004] indicate that crustal contamination played an important role in the genesis of the Jinchuan ultramafic intrusion. It has been suggested that crustal contamination of basaltic magma could be the primary cause for the formation of the world's major magmatic Ni-Cu sulfide deposits, because it either introduced additional sulfur, or at least triggered the precipitation of sulfides [*Naldrett*, 1997].

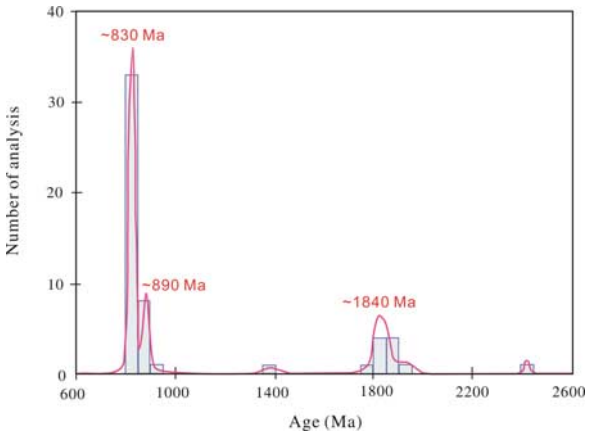

Figure 11. Histogram of SHRIMP U-Pb zircon ages for dolerite dyke and ultramafic rocks from Jinchuan, including data reported by *Li et al.* [2004a]. $^{206}Pb^*/^{238}U$ and $^{207}Pb^*/^{206}Pb^*$ ages are used for zircons younger and older than 1000 Ma, respectively. Age of ~830 Ma is the timing of crystallization of the ultramafic intrusion and the dolerite dyke, and others are inherited zircon ages that document a magmatic event at ~890 Ma and a metamorphic event at ~1840 Ma.

[25] Despite the fact that major world-class magmatic Ni-Cu-PGE sulfide deposits could be formed in distinct tectonic settings such as Archean greenstone belts, rifted continental margins, and intracontinental environments [*Naldrett*, 1997], most of them are genetically related to magmas of mantle plume origin, including continental flood basalts (i.e., Noril'sk-Talnakh and Duluth), komatiites (i.e., Kambalda and Thompson Belt) and large layered mafic-ultramafic complexes (i.e., Bushveld and Great Dyke of Zimbabwe). The Jinchuan intrusion was previously considered as being generated at a Mesoproterozoic rifted continental margin [*Chai and Naldrett*, 1992a, 1992b; *Naldrett*, 1997]. However, our new SHRIMP U-Pb age results indicates that the Jinchuan ultramafic intrusion along with the Ni-Cu sulfide deposit was crystallized in the Neoproterozoic, rather than the Mesoproterozoic.

[26] Because there is no evidence for Neoproterozoic rifting and rift-related magmatism in North China craton [e.g., *Grimmer et al.*, 2003], two questions arise about the genesis of the Jinchuan ultramafic intrusion. (1) Was the Jinchuan intrusion located in the southwestern margin of the North China craton as previously thought? (2) What kind of tectonic regime was responsible for its formation?

[27] The Longshoushan terrane is bounded by faults between the Alxa massif (westernmost North China craton) and the northern Qilian Orogenic Belt (Figure 1b); thus its tectonic affinity is yet to be clearly determined. Inherited U-Pb zircon ages of the Jinchuan ultramafic intrusion and dolerite dyke help to determine if it was tectonically akin to the North China craton or the Qilian in the Neoproterozoic, since accretion of the Qaidam and Qilian terranes to the North China craton occurred during Silurian-Devonian time [e.g., *Yin and Harrison*, 2000]. Compilation of U-Pb zircon ages [*Grimmer et al.*, 2003] shows that the North China craton was characterized by intensive magmatism at ~2.5 Ga along with subordinate magmatic events at 1.7–1.9 Ga, 2.8–3.4 Ga and ~3.8 Ga, and a major period of magmatic quiescence during 1.6–0.6 Ga. In contrast, three major episodes of magmatism are documented at ~1.0 Ga, 920–930 Ma and ~840 Ma in the Qaidam and Qilian terranes [*Gehrels et al.*, 2003a; *Lu et al.*, 2003]. In addition, detrital zircons from the Meso- to Neo-Proterozoic sedimentary strata of the Qilian and Qaidam terranes yield ages of 820–930 Ma, 1.1–1.9 Ga and 2.3–2.6 Ga [*Gehrels et al.*, 2003b], with the young zircons interpreted as being from local igneous rocks. In comparison with the above U-Pb zircon chronological frameworks in the North China craton and Qaidam-Qilian terranes, U-Pb zircon ages from Jinchuan, particularly the two major episodes of magmatism at ~900 Ma and ~830 Ma (Figure 11), are comparable with those in the Qaidam-Qilian terranes, but clearly distinct from those in North China craton. Thus the Jinchuan magmatic rocks (and the Longshoushan terrane as well) are most likely akin to the Qaidam and Qilian terranes, rather than the North China craton. This interpretation is consistent with geophysical results that the Longshoushan terrane was a northward thrust nappe during amalgamation of the Qilian-Qaidam and North China [*Shi et al.*, 1995].

[28] The Qilian Orogenic Belt is generally considered as the western extension of the Qinling Orogenic belt [e.g., *Yang et al.*, 2003; *Song et al.*, 2003] that was once the northern part of the Yangtze craton [e.g., *Ratschbacher et al.*, 2003], since these two belts experienced a coherent tectonic history during the Neoproterozoic and Paleozoic [e.g., *Yang et al.*, 2003; *Gehrels et al.*, 2003a; *Lu et al.*, 2003; *Ling et al.*, 2003; *Su et al.*, 2004]. Hence the Qaidam and Qilian, as well as the Longshoushan terrane (including the Jinchuan pluton), were most likely part of the "Greater South China Block" [*Cheng*, 1994] in the early Neoproterozoic.

[29] The first phase of Neoproterozoic intraplate magmatism in the Yangtze craton started at 830–820 Ma, which was likely triggered by a ~825 Ma mantle plume beneath south China [*Li et al.*, 1999; *Li et al.*, 2003]. It is noticeable that the Jinchuan dolerite and ultramafic intrusion are identical in age to the plume-induced mafic dykes of 827–828 Ma in northern Guangxi of south China and neighboring Australia [*Zhao et al.*, 1994; *Wingate et al.*, 1998; *Li et al.*, 1999]. They are also coeval with the plume-related Tiechuanshan tholeiites [*Ling et al.*, 2003] in the Hannan region of northwestern Yangtze craton. Synchronous mafic to ultramafic intrusions have also been documented in the Yangtze craton, such as the ~820 Ma Hannan complex with V-Ti mineralization [*Zhou et al.*, 2002; *Su*, 2004] and the ~820–840 Ma Tongde-Gaojiacun complex with Ni-Cu-PGE mineralization [*Zhu et al.*, 2004]. Therefore we interpret that the ~825 Ma south China mantle plume was responsible for the Jinchuan Ni-Cu sulfide-bearing ultramafic intrusion, an origin that resembles that of many other world-class magmatic Ni-Cu sulfide deposits of plume origin.

6. Conclusions

[30] New SHRIMP U-Pb zircon and baddeleyite dating results confirm that the Jinchuan ultramafic intrusion formed at ~825 Ma. Integrated mineralogical, petrological and geochemical data are all consistent with an anomalously hot, mantle plume origin for the ultramafic intrusion, although crustal contamination played an important role in its genesis. The Jinchuan mafic-ultramafic rocks not only show a tectonic affinity to the South China Block, based on SHRIMP U-Pb ages of both baddeleyites and zircons of igneous and inherited origin, but are also coeval with the plume-related mafic dykes, tholeiites and mafic-ultramafic complexes with associated V-Ti and Ni-Cu-PGE mineralization in south China. Therefore formation of the Jinchuan ultramafic intrusion and associated Ni-Cu sulfide deposit was likely caused by the ~825 Ma south China mantle plume.

Acknowledgments

[31] We thank X. H. Zhang and R. F. Jiang for assistance in fieldwork, X. L. Tu for trace element analysis, and X. R. Liang for Nd isotope analysis. Comments by Shen-su Sun and Kent C. Condie on early versions of the manuscript were helpful. M. T. D. Wingate kindly provides the baddeleyite reference PBR2. The paper has benefited from constructive review comments of Bin Chen, Antony Naldrett, and Yoshiyuki Tatsumi and editorial comments of William M. White. X.H.L. thanks the NSC (Taiwan) for providing a four-month visiting fellowship to the National Taiwan University. This work is supported by the NSFC (grants 40421303 and 40273012) and the Chinese Academy of Sciences (GIGCX-04-06). This is Tectonics Special Research Centre publication 318, a contribution to IGCP 440.

References

Barnes, S. J., and Z. L. Tang (1999), Chrome spinel from the Jinchuan Ni-Cu sulfide deposit, Gansu Province, People's Republic of China, *Econ. Geol.*, *94*, 343–356.

Black, L. P., S. L. Kamo, C. M. Williams, R. Mundil, D. W. Davis, R. J. Korsch, and C. Foudoulis (2003), The application of SHRIMP to Phanerozoic geochronology: A critical appraisal of four zircon standards, *Chem. Geol.*, *200*, 171–181.

Cabanis, B., and M. Lecolle (1989), Le diagramme La/10–Y/15–Nb/8: Un outil pour la discrimination des series volcaniques et la mise en evidence des procesus de melange et/ou de contamination crutale, *C. R. Acad. Sci. Ser. II*, *309*, 2023–2029.

Chai, G., and A. J. Naldrett (1992a), Characteristics of Ni-Cu-PGE mineralization and genesis of the Jinchuan deposit, northwest China, *Econ. Geol.*, *87*, 1475–1495.

Chai, G., and A. J. Naldrett (1992b), The Jinchuan ultramafic intrusion: Cumulate of a high-Mg basaltic magma, *J. Petrol.*, *33*, 277–304.

Chen, B., B.-M. Jahn, K. Ye, and J. B. Liu (2002), Cogenetic relationship of the Yangkouo gabbro-to-granite unit, Su-Lu terrane, eastern China, and implications for UHP metamorphism, *J. Geol. Soc. London*, *159*, 457–467.

Cheng, Y. Q. (Ed.) (1994), *Outline of Regional Geology of China*, 517 pp., Geol. Publ. House, Beijing.

Chesley, J. T., and J. Ruiz (1998), Crust-mantle interaction in large igneous provinces: Implications from the Re-Os isotope systematics of the Columbia River flood basalts, *Earth Planet. Sci. Lett.*, *154*, 1–11.

Compston, W., I. S. Williams, and C. Meyer (1984), U-Pb geochronology of zircons from lunar breccia 73217 using a sensitive high mass-resolution ion microprobe, *Proc. Lunar Planet. Sci. Conf. 14th*, Part 2, *J. Geophys. Res.*, *89*, suppl., B525–B534.

DePaolo, D. J. (1981), Trace element and isotopic effects of combined wall-rock assimilation and fractional crystallization, *Earth Planet. Sci. Lett.*, *53*, 189–202.

Gao, S., W. Ling, Y. Qiu, L. Zhou, G. Hartmann, and K. Simon (1999), Contrasting geochemical and Sm-Nd isotopic compositions of Archean metasediments from the Kongling high-grade terrain of the Yangtze craton: Evidence for cratonic evolution and redistribution of REE during crustal anatexis, *Geochim. Cosmochim. Acta*, *63*, 2071–2088.

Gehrels, G. E., A. Yin, and X. Wang (2003a), Magmatic history of the northeastern Tibetan Plateau, *J. Geophys. Res.*, *108*(B9), 2423, doi:10.1029/2002JB001876.

Gehrels, G. E., A. Yin, and X. F. Wang (2003b), Detrital-zircon geochronology of the northeastern Tibetan plateau, *Geol. Soc. Am. Bull.*, *115*, 881–896.

Grimmer, J. C., L. Ratschbacher, M. McWilliams, L. Franz, I. Gaitzsch, M. Tichomirowa, B. R. Hacker, and Y. Zhang (2003), When did the ultrahigh-pressure rocks reach the surface? A $^{207}Pb/^{206}Pb$ zircon, $^{40}Ar/^{39}Ar$ white mica, Si-in-white mica, single-grain provenance study of Dabie Shan synorogenic foreland sediments, *Chem. Geol.*, *197*, 87–110.

Gruau, G., J. Bernard-Griffiths, and C. Lecuyer (1998), The origin of U-shaped rare earth patterns in ophiolite peridotites: Assessing the role of secondary alteration and melt/rock reaction, *Geochim. Cosmochim. Acta*, *62*, 3545–3560.

Heaman, L. M., and A. N. LeCheminant (1993), Paragenesis and U-Pb systematics of baddeleyite (ZrO2), *Chem. Geol.*, *110*, 95–126.

Humayun, M., L. P. Qin, and M. D. Norman (2004), Geochemical evidence for excess iron in the Hawaiian mantle: Implications for mantle dynamics, *Science*, *306*, 91–94.

Lee, C. T. (2004), Are Earth's core and mantle on speaking terms?, *Science*, *306*, 64–65.

Li, C., Z. Xu, S. A. De Waal, E. M. Ripley, and W. D. Maier (2004), Compositional variations of olivine from the Jinchuan Ni-Cu sulfide deposit, western China: Implications for ore genesis, *Miner. Deposita*, *39*, 159–172.

Li, X. H., Z. X. Li, W. Ge, H. Zhou, W. Li, Y. Liu, and M. T. D. Wingate (2003), Neoproterozoic granitoids in South China: Crustal melting above a mantle plume at *ca*.825 Ma?, *Precambrian Res.*, *122*, 45–83.

Li, X. H., L. Su, B. Song, and D. Y. Liu (2004a), SHRIMP U-Pb zircon age of the Jinchuan ultramafic intrusion and its geological significance, *Chin. Sci. Bull.*, *49*, 420–422.

Li, X. H., D. Y. Liu, M. Sun, W. X. Li, X. R. Liang, and Y. Liu (2004b), Precise Sm-Nd and U-Pb isotopic dating of the super-giant Shizhuyuan polymetallic deposit and its host granite, Southeast China, *Geol. Mag.*, *141*, 225–231.

Li, Z. X., X. H. Li, P. D. Kinny, and J. Wang (1999), The breakup of Rodinia: Did it start with a mantle plume beneath South China?, *Earth Planet. Sci. Lett.*, *173*, 171–181.

Ling, W. L., S. Gao, B. R. Zhang, H. M. Li, Y. Liu, and J. P. Cheng (2003), From subduction zone to intracontinental rifting: Neoproterozoic tectonic setting conversion along the northwestern margin of Yangtze craton, South China, *Precambrian Res.*, *122*, 111–140.

Lu, S. N., H. K. Li, and Z. H. Chen (2003), Characteristics, sequence and ages of Neoproterozoic thermo-tectonic events between Tarim and Yangzi blocks: A hypothesis of Yangzi-Tarim connection (in Chinese with English abstract), *Earth Sci. Frontiers*, *10*, 321–326.

McKenzie, D., and M. H. Bickle (1988), The volume and composition of melt generated by extension of the lithosphere, *J. Petrol.*, *29*, 625–679.

McKenzie, D., and R. K. O'Nions (1991), Partial melt distributions from inversion of rare earth element concentration, *J. Petrol.*, *32*, 1021–1091.

Naldrett, A. J. (1997), Key factors in the genesis of Noril'sk, Subdury, Jinchuan, Voisey's Bay and other world-class Ni-Cu-PGE deposits: Implications for exploration, *Aust. J. Earth Sci.*, *44*, 283–316.

Naldrett, A. J. (1999), World-class Ni-Cu-PGE deposits: Key factors in their genesis, *Miner. Deposita*, *34*, 227–240.

Norman, M. D., and M. O. Garcia (1999), Primitive magmas and source characteristics of the Hawaiian plume: Petrology and geochemistry of shield picrites, *Earth Planet. Sci. Lett.*, *168*, 27–44.

Ratschbacher, L., B. R. Hacker, A. Calvert, L. E. Webb, J. C. Grimmer, M. O. McWilliams, T. Ireland, S. W. Dong, and J. M. Hu (2003), Tectonics of the Qinling (Central China): Tectonostratigraphy, geochronology, and deformation history, *Tectonophysics*, *366*, 1–53.

Russell, J. K., and J. Nicholls (1988), Analysis of petrologic hypotheses with Pearce element ratios, *Contrib. Mineral. Petrol.*, *99*, 25–35.

Sixth Geological Unit of the Gansu Geological Survey (SGU) (1984), *Geology of Baijiazuizi Ni-Cu Deposit*, 225 pp., Geol. Publ. House, Beijing.

Shi, Y. J., C. W. Zhang, and S. C. Cun (1995), Identification of the Longshoushan nappe and its geological significance (in Chinese), *Chi. Sci. Bull.*, *40*, 812–813.

Shirey, S. B., and R. J. Walker (1998), The Re-Os isotope system in cosmochemistry and high-temperature geochemistry, *Annu. Rev. Earth Planet. Sci.*, *26*, 423–500.

Song, S. G., J. S. Yang, Z. Q. Xu, J. G. Liou, C. L. Wu, and R. D. Shi (2003), Metamorphic evolution of coesite-bearing UHP terrane in the North Qaidam, northern Tibet, NW China, *J. Metamorph. Geol.*, *21*, 631–644.

Stacey, J. S., and J. D. Kramers (1975), Approximation of terrestrial lead isotope evolution by two-stage model, *Earth Planet. Sci. Lett.*, *26*, 207–221.

Su, L. (2004), Studies of Neoproterozoic mafic and ultramafic intrusions in western-central China and their constraints on breakup of Rodinia supercontinent, Ph.D. thesis, 107 pp., Northwest Univ., Xi'an, China.

Su, L., S. G. Song, B. Song, D. W. Zhou, and J. R. Hao (2004), SHRIMP zircon U-Pb ages of garnet pyroxenite and Fushui gabbroic complex in Songshugou region and constraints on tectonic evolution of Qinling Orogenic Belt, *Chin. Sci. Bull.*, *40*, 1307–1310.

Sun, S. S., and W. F. McDonough (1989), Chemical and isotopic systematics of oceanic basalt: Implications for mantle composition and processes, in *Magmatism in the Ocean Basins*, edited by A. D. Saunders and M. J. Norry, *Geol. Soc. Spec. Publ.*, *42*, 313–345.

Tang, Z., and W. Li (1995), *The Metallogenetic Model and Geological Contrast of the Jinchuan Platinum-Bearing Ni-Cu Sulfide Deposit*, 209 pp., Geol. Publ. House, Beijing.

Tang, Z., J. Yang, S. Xu, X. Tao, and W. Li (1992), Sm-Nd dating of the Jinchuan ultramafic rock body, Gansu, China, *Chin. Sci. Bull.*, *37*, 1988–1991.

Williams, I. S. (1998), U-Th-Pb geochronology by ion microprobe, *Rev. Econ. Geol.*, *7*, 1–35.

Wingate, M. T. D., and W. Compston (2000), Crystal orientation effects during ion microprobe U-Pb analysis of baddeleyite, *Chem. Geol.*, *168*, 75–97.

Wingate, M. T. D., I. H. Campbell, W. Compston, and G. M. Gibson (1998), Ion microprobe U-Pb ages for Neoproterozoic-basaltic magmatism in south-central Australia and implications for the breakup of Rodinia, *Precambrian Res.*, *87*, 135–159.

Yang, G., A. Du, W. Qu, J. Chen, G. Yu, and Z. Peng (2004), Pt-Os and Re-Os dating of ores from the Jinchuan Ni-Cu-PGE deposit, a world class Ni deposit, paper presented at Goldschmidt 2004, Eur. Assoc. for Geochem., Copenhagen.

Yang, J., Z. Xu, L. F. Dobrzhinetskaya, H. W. Green II, X. Pei, R. Shi, C. Wu, J. L. Wooden, J. Zhang, Y. Wan, and H. Li (2003), Discovery of metamorphic diamonds in central China: An indication of a >4000-km-long zone of deep subduction resulting from multiple continental collisions, *Terra Nova*, *15*, 370–379.

Yin, A., and T. M. Harrison (2000), Geologic evolution of the Himalayan-Tibetan orogen, *Annu. Rev. Earth Planet. Sci.*, *28*, 211–280.

Zhao, J. X., M. T. McCulloch, and R. J. Korsch (1994), Characterisation of a plume-related ~800 Ma magmatic event and its implications for basin formation in central-southern Australia, *Earth Planet. Sci. Lett.*, *121*, 349–367.

Zhou, M. F., A. K. Kennedy, M. Sun, J. Malpas, and C. M. Lesher (2002), Neoproterozoic arc-related mafic intrusions

along the northern margin of South China: Implications for the accretion of Rodinia, *J. Geol.*, *110*, 611–618.

Zhu, W., H. Deng, B. Liu, C. Li, Y. Qin, Y. Luo, Z. Li, and D. Pi (2004), The age of the Gaojiacun mafic-ultramafic intrusive complex in the Yanbian area, Sichuan Province: Geochronological constraints by U-Pb dating of single zircon grains and $^{40}Ar/^{39}Ar$ dating of hornblende, *Chin. Sci. Bull.*, *49*, 1077–1085.